

Rapid, Sensitive and Real-Time Multiplexing Platform for the Analysis of Protein and Nucleic-Acid Biomarkers

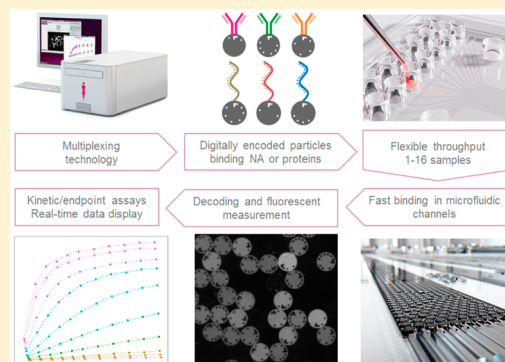
Didier Falconnet,^{*,†} Joseph She,[†] Raphaël Tornay,[†] Elisa Leimgruber,[†] David Bernasconi,[†] Lucienne Lagopoulos,[†] Philippe Renaud,[‡] Nicolas Demierre,[†] and Patrick van den Bogaard[†]

[†]MyCartis, EPFL Innovation Park G, 1015 Lausanne, Switzerland

[‡]Laboratoire de Microsystèmes (LMIS4), École Polytechnique Fédérale de Lausanne (EPFL), 1015 Lausanne, Switzerland

S Supporting Information

ABSTRACT: We describe a multiplexing technology, named Evaluation, based on novel digitally encoded microparticles in microfluidic channels. Quantitative multiplexing is becoming increasingly important for research and routine clinical diagnostics, but fast, easy-to-use, flexible and highly reproducible technologies are needed to leverage the advantages of multiplexing. The presented technology has been tailored to ensure (i) short assay times and high reproducibility thanks to reaction-limited binding regime, (ii) dynamic control of assay conditions and real-time binding monitoring allowing optimization of multiple parameters within a single assay run, (iii) compatibility with various immunoassay formats such as coflowing the samples and detection antibodies simultaneously and hence simplifying workflows, (iv) analyte quantification based on initial binding rates leading to increased system dynamic range and (v) high sensitivity via enhanced fluorescence collection. These key features are demonstrated with assays for proteins and nucleic acids showing the versatility of this technology.



Diagnosis of complex diseases and response to treatments are often associated with multiple biomolecules rather than a single identifiable biomarker. Therefore, understanding disease progression or therapy response requires interrogating a set of biologically relevant biomarkers. In contrast to conventional techniques, multiplexing technologies have rendered this task much more efficient. Within a single assay, tens to thousands of different biomolecules, e.g., proteins or nucleic acids, can be measured from a single sample using identical conditions.^{1,2} The power of these technologies has massively increased the density of information per sample volume and consequently decreased the cost per data point. Multiplexing technologies also enable studies that are difficult to perform with traditional single analyte or low-plexing techniques, e.g., ELISA, standard qPCR, due to limited sample availability.^{1,3}

These undisputed advantages have made multiplexing technologies ubiquitous to many research laboratories and clinical settings.

Various multiplexing technologies are commercially available or at proof-of-concept level. Each technology can be classified according to its specific encoding strategy.⁴ Bead-based technologies (xMAP^{5,6} and digital ELISA^{7,8}) are based on spectral encoding in which the color and intensity allows discriminating each bead population. Planar arrays^{9,10} rely on *x*–*y*-coordinates of the capture spots. Nanostring¹¹ encodes reporter probes via strings of fluorescent segments where the position and color of each fluorescent segment constitutes a

barcode corresponding to a unique target molecule. Alternatively, barcodes have also been embedded into carriers supporting the capture molecules. For example, stop-flow lithography uses UV to polymerize hydrogel enabling simultaneous particle synthesis, functionalization and barcoding in a single step.^{12,13} Barcodes have also been applied to metallic microrods,¹⁴ magnetic and polymer-based particles.^{15,16}

Each encoding strategy generally requires dedicated setups for reaction and/or readout. Each system has inherent performance limitations such as multiplexing level, sensitivity, encoding robustness, operation complexity and reproducibility.^{9,17,3,4} The most popular commercially available multiplexing technologies are bead- and array-based.^{1,18} Due to their wide adoption and ability to measure proteins and nucleic acids these two technologies are discussed in further details.

High spot densities of planar arrays are ideal tools for screening thousands of biomolecules on a single slide. They have been proven to be valuable for gene expression profiling¹⁹ or identifying autoantibodies²⁰ and numerous other applications. However, irrespective of the spot density, the panel of the capture molecules needs to be predefined before array manufacturing, making the system inflexible to assay developers who require testing of many probe variants for optimization and with a rapid iteration cycle. Heath et al. proposed a method

Received: July 11, 2014

Accepted: January 7, 2015

Published: January 7, 2015

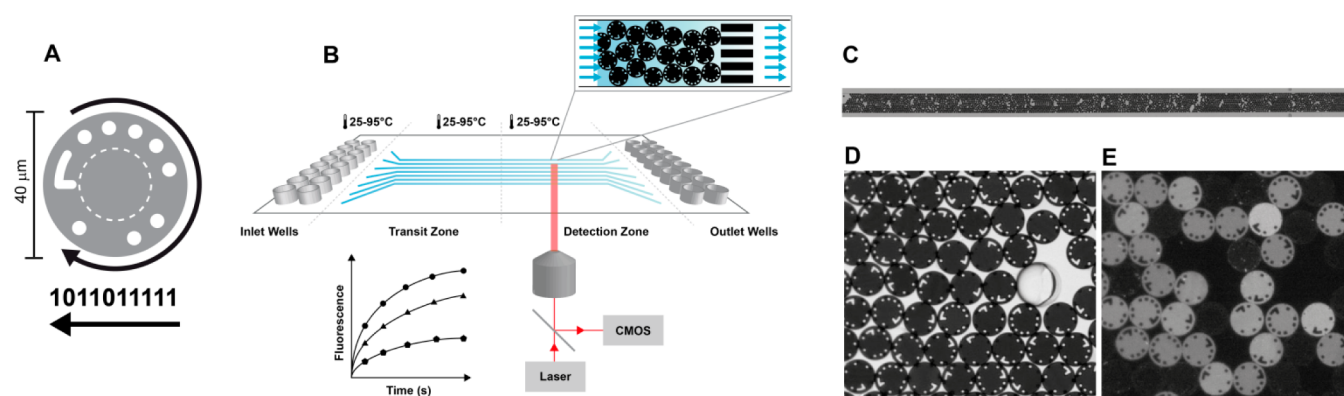


Figure 1. Schematics of the technology. (A) The digitally encoded microparticle are silicon discs (diameter of 40 μm and thickness of 10 μm) with 10 binary coding bits on their periphery enabling 1024 (2^{10}) different codes. An “L” shaped mark is used for particle orientation and decoding starting bit. The arrow indicates the decoding direction and is done via automated detection of the presence or absence of a hole at the 10 possible locations. The central area is dedicated to fluorescence intensity measurement (approximately 1800 pixels per particle). (B) The cartridge is composed of 16 independent microfluidic channels. The instrument interfacing the cartridge enables temperature control between 25 and 95 $^{\circ}\text{C}$ in 3 zones: the inlet wells, the transit and the detection zone. Samples and all necessary reagents are delivered (premixed or sequentially) from the inlet wells to the capturing particles by a pressure differential (0–2000 mbar) enabling fast binding kinetics. The particles are retained static in the microchannel by a filter structure allowing the samples and reagents to flow over and around while keeping them static. A single or multiple channels can be optically scanned during the assay either as a time lapse or end point acquisition. Images are processed on-the-fly providing real-time data display. (C) Stitched bright-field images of a channel filled with a monolayer of approximately 3000 microparticles (corresponding to a plug of 12 mm scanned with 14 fields of view). (D) Section of a bright-field (BF) image used for automated decoding. The transparent circular feature is a supporting post to guarantee accurate channel height. (E) Corresponding fluorescent image used for automated analyte quantification.

of DNA-encoded antibody libraries that may improve flexibility of array usage.^{21,22} In contrast, bead-based technologies have proven to be highly flexible and scalable. They allow users to couple different capture molecules on different bead sets and mix the selected populations to easily adapt the multiplex panel to their specific needs.¹³ However, the currently available bead-based systems are designed to run cost-effectively in batches (typically 96 wells) and the need for waiting on sufficient samples to fill the plate can slow down the turnaround time (time-to-result) in routine clinical testing.

Furthermore, both technologies (planar arrays and bead-based systems) suffer from slow binding kinetics, as they are mainly driven by diffusion.²³ This usually imposes long sample incubation times (from several hours to overnight) even when agitation is used to speed up the process. In addition, diffusion-limited binding regime can also contribute to reported high intra- and interassay variations.^{3,13,24,25}

We set out to develop the Evaluation system, a flexible technology amenable to mass-production and addressing the above limitations as well as providing means to shortening assay development time. These goals steered the development of three key features: A novel type of digitally encoded microparticles for robust and flexible multiplexing. An assay plate with an adaptable throughput (no batching required) composed of independent microfluidic channels^{26,27} for reproducible²⁸ and fast binding kinetics.²³ An instrument interfacing the assay plate and providing dynamic control over assay conditions and real-time data processing and display.

This paper first describes the encoded microparticles, the fluidic cartridge and the integration with the instrument functionalities. In the Results section, we demonstrate binding in reaction-limited regime corresponding to maximal achievable binding rates and accountable for short assay time. A number of multiplexed protein and nucleic acid assays are quantified in end point or in kinetic mode to demonstrate the flexibility (dynamic assay control and real-time readout), sensitivity and reproducibility of this technology.

EXPERIMENTAL SECTION

The challenges in technology transfer from proof-of-concept to industry products can arguably be measured by the discrepancy between the number of publications on lab-on-chip systems and commercially available platforms.²⁶ A fundamental requirement for the development of this technology was therefore that the components (particles, cartridges and instrumentation) would be amenable to mass-production processes.

Encoded Microparticles. The central components of the Evaluation technology are the disc-shaped digitally encoded silicon microparticles (Figure 1A,D,E). The periphery is dedicated to the encoding using 10 binary bits (presence or absence of a hole). This encoding strategy is robust, as the holes physically go through the microparticle thickness and thus cannot be altered by light-induced damage or chemical degradation.

The encoded particles act as solid support for tethered capture molecules such as antibodies, antigens, peptides, nucleic acid probes or other biomolecules. Fluorescence is used for readout. The particles are coated with an optical enhancement layer inducing constructive interference of the fluorophores emitted light.^{29,30} Multiple particles sharing an identical code form a population and provide measurement redundancy for statistical confidence. The Supporting Information provides details about manufacturing and particle redundancy.

Microfluidic Cartridges. The cartridge, or assay plate (Figure 1B), features 16 microscale channels hosting the microparticle mixes and enabling running from 1 to 16 samples simultaneously or sequentially (i.e., at different dates). Each channel connects an inlet well (for input volumes between 5 and 130 μL) and a waste reservoir (200 μL). The volume of a channel is approximately 700 nL. Each microchannel is 400 μm wide and includes a filter structure to restrain the microparticles in the detection zone. The height of the channels (16 μm) is optimized for efficient microparticle loading and tiling. The

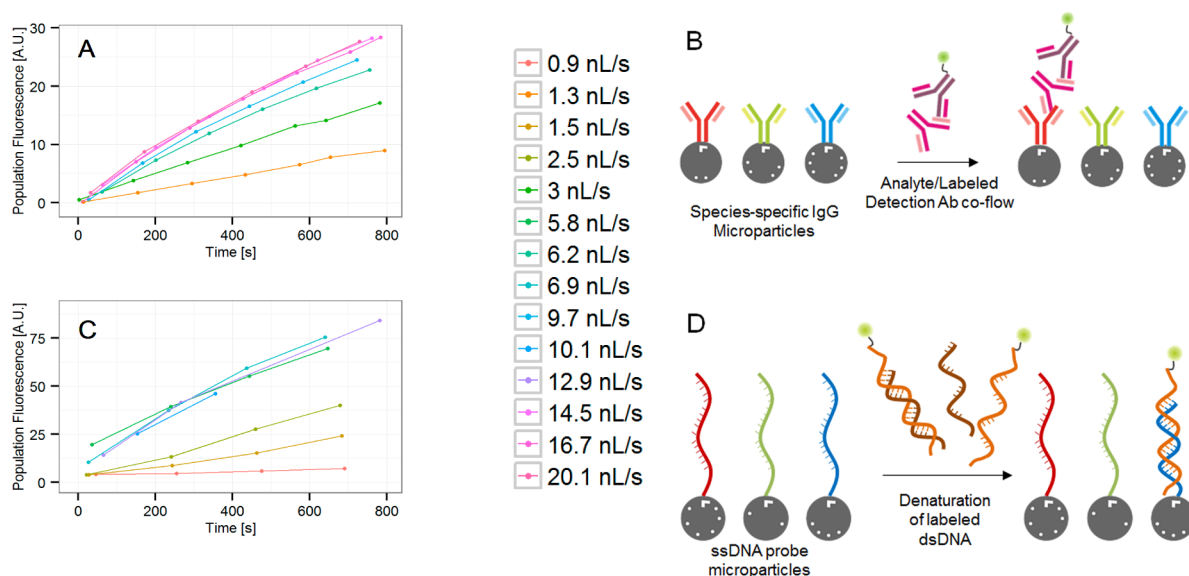


Figure 2. Reaction-limited regime vs mass transport-limited regime for 2 model assays. (A) Fluorescence signal increase in function of time for different flow rates in the case of an antibody detection in a coflow format as described in panel B. Coflow assay format: the sample-containing analyte, here an antibody (goat antirabbit IgG), is premixed with the fluorescently labeled detector antibody (Dylight647 donkey antigoat IgG) prior to be flowed in the channel. Panel C represents double-stranded nucleic acid (RSVA) detection as illustrated in panel D. For both assays (antibody capture and DNA hybridization), the kinetic curves in panels A and C overlap when a certain flow rate threshold is past. Operating above the threshold implies reaction limited regime where binding rate is maximal and becomes independent of flow rate. Below the threshold, reactions become slower and display an undesired dependency with flow rate. The threshold for reaction limited regime in panel A is at approximately 13 nL/s and approximately 6 nL/s in panel C. A total of approximately 250 particles (i.e., 1 mm plug length) was loaded per channel, and the applied differential pressures ranged from 10 to 200 mbar. The relationship between the total number of particles, the applied pressure and the resulting flow rate can be found in the Supporting Information.

shallow channel height prevents microparticles from overlapping each other.

The monolayer arrangement of microparticles in the channel enables the use of high resolution imaging for both decoding and fluorescence quantification (see the Supporting Information for details). Loading is performed in a semiautomated fashion using a pumping device that interfaces with the cartridge. Each channel can be loaded with up to 3000 microparticles corresponding to a total loading length of 12 mm (Figure 1C). A fully loaded channel enables a multiplexing level of up to 150 with 20 particles per population (see the Supporting Information for details). Cartridges are mass-produced by injection molding of cyclo-olefin copolymer (COC) and provide high quality optical properties as well as minimal nonspecific biomolecule adsorption.³¹ The footprint complies with microtiter plate format (SBS standards) compatible with laboratory automation such as robotic arms and liquid handling systems.

Instrument. The benchtop instrument has three main functions: imaging the particles in bright field and fluorescence, fluid actuation and temperature control.

The optical system is designed around a 10× long-working distance objective (NA 0.3) and a high-sensitivity CMOS camera to acquire bright field and epi-fluorescence images (excitation at 640 nm). The objective is mounted on an automated *x-y-z* stage for scanning each channel either during the assay for real-time readout or in end point. The particles are imaged from the bottom of the cartridge. Decoding is entirely decoupled from the binding quantification as they are respectively performed in bright field (Figure 1D) and fluorescence imaging mode (Figure 1E). Bright field and fluorescence images are taken consecutively so that the relative

position of each particle is the same in both images. Image processing is performed in real-time to detect particles, read codes, quantify fluorescence, compute aggregate values for each population (see the Supporting Information for details) and display data.

Liquids (sample, buffer and other assay reagents) are pushed through the channels by application of a pressure differential between the inlet and outlet wells. Moreover, both inlets and outlets are pressurized above atmospheric pressure to provide robust microfluidic operation and effectively prevent formation of bubbles — an often encountered problem in microfluidic systems. Each of the 16 channels is controlled individually for pumping/no pumping state. However, the applied pressure differential is the same for all channels. Flow rates are calibrated for pressure difference and number of particles via a simple linear function of the pressure and fluidic conductance (see the Supporting Information for details).

Temperature is controlled with Peltier elements in 3 independent zones, and each can be set independently between 25 and 95 °C (Figure 1B and the Supporting Information): (i) the detection zone containing the particles where the binding reaction is measured (hybridization or affinity capture), (ii) the transit zone typically used for in flow denaturation of double-stranded nucleic acids and (iii) the inlet wells that can be used as a controlled reaction vessel prior to capture on the microparticles. Each temperature zone can be modulated in time according to a user-defined protocol. This flexibility enables running melt-curve analysis or nonstandard test protocols.

Software User Interface. Each subsystem of this technology (i.e., imaging, thermal and fluidic) is controlled by a single interface, allowing user-friendly and flexible edition of

run protocols. The protocols can be modified during the execution of an assay enabling efficient optimization of assay parameters (temperature, binding/wash time, buffer, image acquisition variables) within a single experimental run. Acquired images are processed “on-the-fly”, allowing data to be displayed in real-time, enabling immediate assessment on the impact of the changed assay parameters.

Multiplexed Biological Assays. The panel is prepared by mixing different populations of microparticles, each coupled with a capture molecule of interest (details on coupling protocols can be found in the Supporting Information). Particles from each population are mixed together in equimolar ratios from aliquots containing 20 000 particles of a single population. The mix is then loaded into the microfluidic channel using the dedicated loading device with a multi- or single-channel pipette or a liquid handling system. The cartridge is then inserted into the instrument, and the user-defined protocol is executed.

The procedure for a typical real-time coflow immunoassay or DNA amplicon detection is as follows: Particles are scanned before assay start for determining background fluorescence; buffer is removed from the inlet wells and replaced with samples containing fluorescently labeled detector antibodies or amplicons. This solution is then flowed into the channels and fluorescent signal on microparticles is recorded at repeated time intervals (i.e., kinetically). Procedure for a typical end point sandwich immunoassay, and details about the reagents, assay conditions and bleaching characterization can be found in the Supporting Information.

In Flow Denaturation of Double-Stranded DNA. The temperature controlled transit zone enables in flow double-stranded DNA denaturation³² (Figure 1B). This feature fundamentally contrasts with a closed system (i.e., microwells or microarrays) in which denaturation and hybridization occur within a common location and therefore under a unique temperature. In flow denaturation is advantageous, as the melted double-stranded products flow to the capture probes (detection zone in Figure 1B) within seconds of melting. The reduced time between melting and hybridization limits the extent of reannealing.³² For further details about in flow denaturation, please see the Supporting Information.

Data Analysis and Statistics. Each microparticle fluorescence value is computed from the camera recorded pixels located in the featureless central disc of each microparticle (Figure 1A). The arithmetic mean of microparticles from a population is used to estimate the microparticle population fluorescence (see the Supporting Information for more details).

RESULTS AND DISCUSSION

Reaction Limited Regime for Optimal Binding Kinetics. The active flow through the microfluidic channels provides arguably the most efficient capture environment: The flow guarantees a continuous supply of analytes to the capture molecules and thus largely compensates sample depletion due to surface binding.^{23,24} We demonstrate that for different types of analytes displaced at a sufficient velocity the maximum binding rate is achieved; this is known as reaction limited regime as opposed to mass transport limited regime (also often referred to diffusion limited regime). Figure 2A,C illustrates the effect of flow rate on kinetic binding curves on two representative model assays: a modified antibody capture assay in a coflow format (Figure 2B) and a direct DNA

hybridization assay (Figure 2D). By increasing the flow velocity, the binding rates become higher until curves overlap to a maximum kinetic. The lowest flow rate at which the curves become indistinguishable (i.e., at which curves overlap) defines the smooth transition between reaction- and mass transfer-limited regimes (an alternative view of this regime transition based on the Damköhler number³³ is available in the Supporting Information). Note that both assay types display similar flow rate thresholds for reaction limited regime, demonstrating that the flow rate requirements in this technology can be matched for a variety of analytes (proteins and NA). Operating in the reaction limited regime enables maximum capture rate but it is also critical for analyte quantification. In the reaction limited regime, the fluorescent signal is exclusively dependent on the concentration, allowing quantitation based on fluorescence values. This also releases important technical constraints on the fluidic system in which the need for accurately controlling flow rates is avoided. It is noteworthy that the reaction limited flow rate threshold is independent of the analyte concentration but varies with the molecule affinities and the capture probe surface density.^{23,33} An increased affinity (or probe density) increases the flow rate threshold for reaction limited regime. Therefore, when new assays are being developed one should experimentally verify that the applied flow guarantees reaction limited regime conditions.

Dynamic Control of the Assay Environment and Real-Time Binding Monitoring of Single vs All Targets. Figure 3 illustrates how the dynamic control of the hybridization

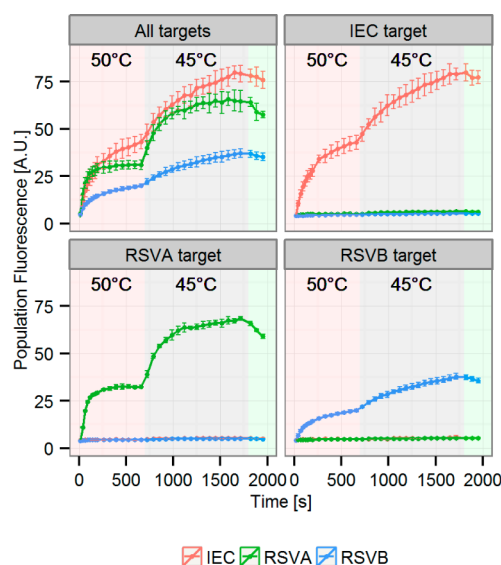


Figure 3. Dynamic control of the hybridization environment with real-time binding monitoring of individual targets vs all targets. Four channels ran in parallel, each loaded with the same 3 microparticle populations. The following protocol was used to demonstrate the ability to change “on-the-fly” assay temperature and buffer while monitoring in real-time hybridization of fluorescently labeled products: (i) 700 s of hybridization at 50 °C monitored in real-time (red background), (ii) subsequent temperature change from 50 to 45 °C while continuously flowing the targets (gray background) and (iii) wash step (i.e., buffer exchange) at ~30 min of total assay time at constant temperature (green background). Single target experiments were used to determine specificity. Double-stranded targets were at 10 nM in 3× SSC buffer and input volumes 60 μL, particle plug length 1 mm and applied pressure difference 200 mbar.

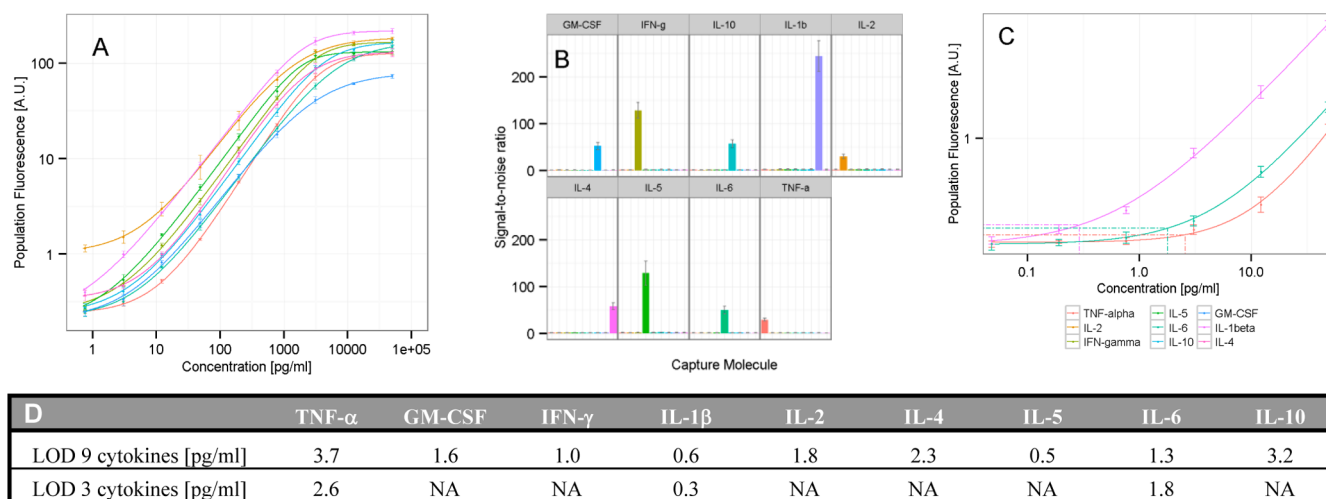


Figure 4. Multiplex cytokine immunoassay in end point format. (A) 9-Plex standard curves across a 5 log concentration range. Error bars represent interassay standard deviations. (B) Cross-reactivity data from the 9 individual cytokines at 100 pg/mL. (C) Subpanel with only 3 cytokines flowed over the 9 particle populations. Dashed lines correspond to the computed limits of detection (mean of blanks+3SD). (D) Limits of detection determined for 9 cytokines flowed simultaneously (independent quadruplicates and 20 blanks) and the subpanel of 3 cytokines (6 independent replicates and 12 blanks). The loaded microparticle plug length were approximately 1.8 mm. 120 μ L of cytokine standard mix was flowed for 60 min followed by 30 min of 50 μ L biotinylated detector antibodies cocktail (40 nM) and 5 min of 35 μ L Alexa647-conjugated streptavidin (75 nM). Applied pressure difference was 300 mbar and temperature controlled for 25 $^{\circ}$ C.

environment can help determining optimal assay conditions within a single assay run. To exemplify this system flexibility, we modified “on-the-fly” the hybridization temperature (50 to 45 $^{\circ}$ C) followed by a buffer change (here a wash step). All changes in binding behaviors were monitored in real-time and multiplex kinetic responses recorded. The DNA probes were designed for detecting the respiratory syncytial virus (RSV), a major cause of lower respiratory tract infections. The target sequences for RSVA, RSVB and IEC (internal extraction control) were adapted from literature.³⁴ The three DNA capture probes were designed for similar probe-target free energies using Visual OMP (DNAsoftware, USA).³⁵ See the Supporting Information, Table S-2 for computed thermodynamic values and assay details.

Parallel channels were used to measure either all targets flowed simultaneously or the individual ones. Fluorescence values were found to be very similar for “all targets” and individual targets, suggesting minimal cross-hybridization. This is supported by small off-target signals or, equivalently, high signal-to-noise ratios (SNR) observed in the single target formats. The SNR was computed as the ratio between the specific signal and the highest nonspecific signal (i.e., fluorescence measured from the off-target particles) when only one target was flowed. At 50 $^{\circ}$ C, the SNR range from approximately 30 for RSVB to approximately 170 for RSVA. When the temperature was decreased from 50 to 45 $^{\circ}$ C, a moderate loss of specificity was observed for RSVA (SNR_{45 $^{\circ}$ C} = 110), whereas no SNR change was observed for the other two species. Such kinetic experiments are by nature in nonwash conditions but nonetheless display high SNR and low fluorescence background.

Differences in reaction rates between the three probe-target pairs can readily be identified on the multiplex kinetic curves (Figure 3, “All targets”). RSVA rapidly reaches equilibrium, whereas RSVB and IEC display a residual positive slope at 700 s, indicating that the reactions have not yet reached equilibrium. Such kinetic plots also allow easy identification of probes that should undergo design iteration; depending on the required

assay performances one may want to increase for example the affinity of RSVB.

Lowering the temperature to 45 $^{\circ}$ C while still flowing the targets induces a shift toward a new equilibrium with increased binding affinity and consequently higher fluorescent signals and limited effect on specificity.

The experimental fluorescence values obtained for the 3 targets near equilibrium are, from highest to lowest, IEC, RSVA and RSVB. This ranking was predicted by the computed hybridization free energies indicating a concordance between in-silico and experimental results. The demonstration protocol was finalized with a wash step at 45 $^{\circ}$ C (green area in Figure 3) highlighting the possibility to access dissociation constants. The kinetic wash can also be used for optimizing the buffer stringency and wash time for achieving the desired specificity.

Human Cytokine Panel, End Point Sandwich Immunoassay. Herein, we demonstrate the straightforward porting of antibodies selected for ELISA assays (see the Supporting Information). Titration, sensitivity and cross-reactivity data are presented.

Multiplexed titrations. We assembled a 9-Plex human cytokine panel with off-the-shelf ELISA antibodies. To evaluate the dose–response relationship, we performed end point multiplexed titrations ranging from 0.048 pg/mL to 50 000 pg/mL (Figure 4A). As expected, each cytokine has a different dose–response curve, e.g., IL-1 β and IFN- γ show saturation at high concentrations whereas IL-6 and IL-10 display no saturation plateau over the range tested. The fluorescence interassay coefficient of variation (CV) over 4 independent repeats (4 cartridges, reagents were freshly prepared each time, and on different days) was found to be as low as 4.8% for TNF- α and 11.9% for IL-2 as average across all tested concentrations including blanks. The interassay CV of the 7 other cytokines were within the above range.

Cross-Reactivity. Cross-reactivity was determined for the 9 cytokines at a clinically relevant concentration (100 pg/mL). Figure 4B shows signal over blank ratio generated by each particle population upon flowing individual cytokines followed

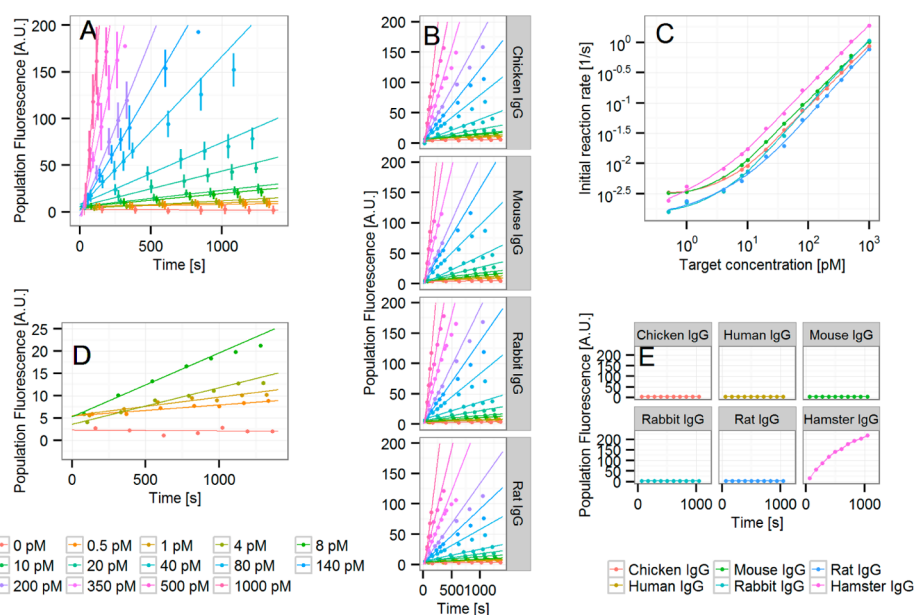


Figure 5. Use of the initial binding rate for determining antibody concentrations with increased dynamic range. The initial binding rates, characterized by the slope of the linear fit (straight line fitting the first 5 data points), were determined on the following multiplex kinetic data: 14 concentrations run in parallel each as a 5-Plex mix of goat antibodies specific to (A) Hamster-IgG, (B) Chicken-IgG, Mouse-IgG, Rabbit-IgG and Rat-IgG coflowed (i.e., premixed) with DyLight647-conjugated donkey antgoat antibody. (C) Standard (calibration) curves for analyte quantitation based on the initial binding rates (color coding is used for each capture antibody population). (D) High resolution plot of (A) highlighting how binding time increases discrimination between similarly low concentrations. (E) Cross-reactivity plot with goat anti-Hamster IgG (80 nM). Loaded microparticle plugs were approximately 2.5 mm, pressure difference applied 500 mbar and temperature controlled for 30 °C.

by a mix of 9 detector antibodies. Cross-reactivity was found to be very low; Signal to blank ratios ranged from ~30- to 250-fold for IL-2 and IL-1 β , respectively. This highlights the good specificity of the antibody pairs and the nonfouling properties of the microparticles.

Sensitivity. Limit of detection (LOD) was determined for the 9-Plex panel and a subpanel of 3 cytokines: TNF- α , IL-1 β and IL-6. Figure 4C shows the fluorescent response of the subpanel at low concentrations (SNR plots can be found in the Supporting Information). The similar limits of detection for both data sets (Figure 4D) indicate that the performance of the assay is not significantly biased by the presence or absence of each analyte. Overall, the resulting sensitivities are better or similar (depending on the cytokine) to values published for competing multiplex technologies.^{36–41} However, the results on the present technology were obtained with significantly shorter time-to-results: approximately 90 min as opposed to typically 5 h (note that for traditional systems overnight incubations are often recommended for optimal performance). Additionally, the hands-on time was only about 30 min. A wide range of complex samples matrices such as serum, saliva and CSF have been used to demonstrate compatibility on Evaluation's microfluidic technology (results will be presented in separate communications).

Kinetic Read-out Expands System Dynamic Range. In a multiplexed environment, analytes are generally present at widely different concentrations and display a range of affinities. Such differences naturally generate a range of signals: typically high fluorescence from highly abundant species and faint signals from molecules at lower concentrations. This potentially large range of signals can in some cases be greater than the sensor dynamic range. In practice, this problem is often solved by measuring multiple dilutions of the sample, so that all analytes have a data point falling within the sensor's dynamic

range. However, this approach is tedious and can only be applied if sufficient sample volume is available, which often defeats the purpose of multiplexing. Matrix interference is also likely to be dilution dependent and may give rise to undesirable dilution bias. To address this limitation we show that (i) the unknown analyte concentration can be determined based on the initial rate of the signal build-up^{42,43} and (ii) that this approach can increase the system dynamic range. Figure 5A displays kinetic data of a model assay in which 14 concentrations of goat antihamster IgG were coflowed with DyLight647-conjugated donkey antgoat antibodies. The dilution series spanned over 3 orders of magnitude (1000 to 0.5 pM), yielding a range of kinetics. The assay was performed in a 5-Plex format, but for readability, each analyte was plotted in a separate figure (Figure 5B). The initial binding rate can be estimated from the slope of the progress curve in its early linear range. For this purpose, a linear fit on the first data points (here, 5 first time points) was performed and the resulting slope extracted. Figure 5C depicts the initial binding rates (i.e., slopes) in function of analyte concentrations which constitute the "kinetic" calibration curves.

Quantification from kinetic curves can be advantageous as it can expand the dynamic range of the system: A high titer sample, e.g., 1000 pM, Figure 5A, under the given assay conditions, leads to camera saturation within minutes (>255 au). As an example, if the assay binding time required for detecting low concentrations is approximately 1000 s (Figure 5D) then the same assay read in an end point format (at 1000 s) would lose the ability to quantitate the analytes between 140 and 1000 pM, as they would saturate the camera and render the data unusable for quantification (Figure 5A). Therefore, in the present assay, quantitating the concentrations with the initial binding rate increases the dynamic range by approximately 1 log. Figure 5E illustrates the specificity of the system through

the coflow of a single analyte (goat antihamster IgG) together with the labeled detector antibody. Note that cross-reactivity was observed between mouse and rat due to species similarity.

System Reproducibility, Data Quality and Number of Microparticles. Reproducibility is arguably the most important aspect for generating reliable quantitative data. We monitored the following 3 system variables: (i) stability of the instrument, (ii) storage stability of the antibody-function-alized microparticles at $-20\text{ }^{\circ}\text{C}$ and (iii) reproducibility of the antibody coupling process. The intent was to characterize the reproducibility of the whole system, i.e., hardware and chemistry, while minimizing contribution from biological variability. We therefore used a simple and robust antibody model assay for minimizing the biological contribution to variability. The total variation obtained when taking into account the above 3 system variables results in a fluorescence CV of 3.8% (a higher granularity in the data and assay methodology can be found in the Supporting Information). Such an overall low coefficient of variation translates into excellent system reproducibility and can, in part, be attributed to a number of technology choices spanning from manufacturing (microparticles and cartridges), chemical coupling protocol and instrument design, e.g., use of a stable laser, all focused toward robustness.

Microfluidic environments are also known to provide well controlled conditions, and thus contribute to the interexperiment data robustness.²⁸ The number of microparticles per population is also to be considered in the context of reproducibility. The minimum number of microparticles required per population is chosen to ensure that the estimated population fluorescence has a high precision and therefore a narrow confidence interval.

The precision of the population fluorescence estimate depends on two factors: microparticle fluorescence variability in the population and the number of microparticles used to compute the population fluorescence (see further details in Supporting Information). From the observed experimental variability across a population, we have concluded that, in general, 10 measured particles per population suffice to obtain a 95% confidence interval for the population fluorescence that has a half width of 12% of the estimated value. In this case, the true population fluorescence is within $\pm 12\%$ of the estimated fluorescence with a probability of 95%. If 50 microparticles are used for the computation of population fluorescence, the 95% confidence interval has a half width of 5% of the estimated value. Therefore, the minimum number of particles required is dependent on desired precision. We also identified that a maximum number of microparticles per population should not be exceeded in order to prevent the formation of a concentration gradient along the channel owing to analyte depletion. Susceptibility to form a gradient is largely dependent on the affinity between the capture and the target molecule, the flow rate and the capture probe surface density. Therefore, a window ranging from 20 to 80 microparticles per population is usually appropriate.

CONCLUSIONS

By leveraging silicon microfabrication techniques and polymer injection methods we developed a mature microfluidic-based multiplexing technology amenable to mass-production.

We demonstrated that with this technology the analyte capture rate is maximized through the use of microfluidic channels operated in the reaction limited regime. This leads to

shorter assay times with competitive analytical sensitivities compared to other multiplexing technologies. Note that the results presented here were generated on a prototype instrument. The system is currently being modified as a commercial system in which a 532 nm laser is installed for enabling the use of bright dyes such as phycoerythrin, ATTO 550 or Alexa Fluor 546. This modification is expected to further improve the sensitivity of this technology.

Dynamic control of assay environment (such as temperature, binding/wash times and image acquisition conditions) and real-time readout can reduce the number of experiments for assay development, and thus enable a broader adoption of multiplexing analysis.

In addition, there is a growing clinical research interest in integrating data from multiple marker types^{44,45} (mRNA, miRNA, DNA and proteins). The ability to quantify them on a single platform is likely to be more cost-effective and beneficial for generating comprehensive and coherent multiplex data sets.

Finally, the flexibility of this technology enables running either traditional sandwich immunoassays (via sequential reagent flow) or coflow assay formats, leading to very simple hands-on procedures. In addition to automated data analysis, the ability to access microparticle images during or after assays provides valuable qualitative information on the assay quality.

We believe the unique ensemble of features of the Evaluation technology makes it a powerful system for biomarker analysis in clinical and translational research.

ASSOCIATED CONTENT

Supporting Information

Supporting Information available as noted in the text. This material is available free of charge via the Internet at <http://pubs.acs.org>.

AUTHOR INFORMATION

Corresponding Author

*D. Falconnet. E-mail: dfalconnet@mycartis.net.

Notes

The authors declare the following competing financial interests: D.F., J.S, R.T, E.L., D.B., L.L., N.D. and P.vB. are MyCartis employees. P.R. is cofounder of MyCartis. P.R., D.F., R.T. and E.L. have financial interests in MyCartis.

ACKNOWLEDGMENTS

The authors thank colleagues that have, through their activities at MyCartis, indirectly participated to the development of the presented Evaluation technology.

REFERENCES

- (1) Ellington, A. a; Kullo, I. J.; Bailey, K. R.; Klee, G. G. *Clin. Chem.* **2010**, *56*, 186–193.
- (2) Spriggs, F. P.; Zhong, Z. D.; Safavi, A.; Jani, D.; Dontha, N.; Kant, A.; Ly, J.; Brilando, L.; Österlund, K.; Rouleau, N.; Fischer, S. K.; Boissonneault, M.; Ray, C. *AAPS J.* **2012**, *14*, 113–118.
- (3) Comley, J. *Drug Discovery World Fall* **2012**, *13*, 23–45.
- (4) Birtwell, S.; Morgan, H. *Integr. Biol.* **2009**, *1*, 345–362.
- (5) Nolan, J. P.; Mandy, F. F. *Cell. Mol. Biol.* **2001**, *47*, 1241–1256.
- (6) Hsu, H.-Y.; Joos, T. O.; Koga, H. *Electrophoresis* **2009**, *30*, 4008–4019.
- (7) Rissin, D. M.; Kan, C. W.; Song, L.; Rivnak, A. J.; Fishburn, M. W.; Shao, Q.; Piech, T.; Ferrell, E. P.; Meyer, R. E.; Campbell, T. G.; Fournier, D. R.; Duffy, D. C. *Lab Chip* **2013**, *13*, 2902–2911.
- (8) Walt, D. R. *Anal. Chem.* **2013**, *85*, 1258–1263.

- (9) Zangar, R. C.; Daly, D. S.; White, A. M. *Expert Rev. Proteomics* **2006**, *3*, 37–44.
- (10) Pozhitkov, A. E.; Tautz, D.; Noble, P. a. *Briefings Funct. Genomics Proteomics* **2007**, *6*, 141–148.
- (11) Geiss, G. K.; Bumgarner, R. E.; Birditt, B.; Dahl, T.; Dowidar, N.; Dunaway, D. L.; Fell, H. P.; Ferree, S.; George, R. D.; Grogan, T.; James, J. J.; Maysuria, M.; Mitton, J. D.; Oliveri, P.; Osborn, J. L.; Peng, T.; Ratcliffe, A. L.; Webster, P. J.; Davidson, E. H.; Hood, L.; Dimitrov, K. *Nat. Biotechnol.* **2008**, *26*, 317–325.
- (12) Pregibon, D. C.; Toner, M.; Doyle, P. S. *Science* **2007**, *315*, 1393–1396.
- (13) Appleyard, D. C.; Chapin, S. C.; Doyle, P. S. *Anal. Chem.* **2011**, *83*, 193–199.
- (14) Walton, I. D.; Norton, S. M.; Balasingham, A.; He, L.; Oviso, D. F.; Gupta, D.; Raju, P. A.; Natan, M. J.; Freeman, R. G. *Anal. Chem.* **2002**, *74*, 2240–2247.
- (15) Lee, H.; Kim, J.; Kim, H.; Kim, J.; Kwon, S. *Nat. Mater.* **2010**, *9*, 745–749.
- (16) Broder, G. R.; Ransinghe, R. T.; She, J. K.; Banu, S.; Birtwell, S. W.; Cavalli, G.; Galitonov, G. S.; Holmes, D.; Martins, H. F. P.; Macdonald, K. F.; Neylon, C.; Zheludev, N.; Roach, P. L.; Morgan, H. *Anal. Chem.* **2008**, *80*, 1902–1909.
- (17) Walt, D. R. *Lab Chip* **2014**, 3195–3200.
- (18) Zhu, H.; Bilgin, M.; Bangham, R.; Hall, D.; Casamayor, a; Bertone, P.; Lan, N.; Jansen, R.; Bidlingmaier, S.; Houfek, T.; Mitchell, T.; Miller, P.; Dean, R. a; Gerstein, M.; Snyder, M. *Science* **2001**, *293*, 2101–2105.
- (19) van't Veer, L. J.; Dai, H.; van de Vijver, M. J.; van der Kooy, K.; Marton, M. J.; Witteveen, A. T.; Schreiber, G. J.; Kerkhoven, R. M.; Roberts, C.; Bernards, A.; Friend, S. H.; Linsley, P. S. *Nature* **2002**, *415*, 530–536.
- (20) Michaud, G. a; Salcius, M.; Zhou, F.; Bangham, R.; Bonin, J.; Guo, H.; Snyder, M.; Predki, P. F.; Schweitzer, B. I. *Nat. Biotechnol.* **2003**, *21*, 1509–1512.
- (21) Bailey, R. C.; Kwong, G. A.; Radu, C. G.; Witte, O. N.; Heath, J. R. *J. Am. Chem. Soc.* **2007**, *129*, 1959–1967.
- (22) Fan, R.; Vermesh, O.; Srivastava, A.; Yen, B. K. H.; Qin, L.; Ahmad, H.; Kwong, G. a; Liu, C.-C.; Gould, J.; Hood, L.; Heath, J. R. *Nat. Biotechnol.* **2008**, *26*, 1373–1378.
- (23) Zimmermann, M.; Delamarche, E.; Wolf, M.; Hunziker, P. *Biomed. Microdevices* **2005**, *7*, 99–110.
- (24) Ng, A. H. C.; Uddayasankar, U.; Wheeler, A. R. *Anal. Bioanal. Chem.* **2010**, *397*, 991–1007.
- (25) Coughlin, C. C.; Bayliss, S. J. *J. Am. Acad. Dermatol.* **2014**, *70*, 197–198.
- (26) Sackmann, E. K.; Fulton, A. L.; Beebe, D. J. *Nature* **2014**, *507*, 181–189.
- (27) Yeo, L. Y.; Chang, H.-C.; Chan, P. P. Y.; Friend, J. R. *Small* **2011**, *7*, 12–48.
- (28) Araz, M. K.; Tentori, A. M.; Herr, A. E. *J. Lab. Autom.* **2013**, *18*, 350.
- (29) Lambacher, A.; Fromherz, P. *Appl. Phys. A: Mater. Sci. Process.* **1996**, *216*, 207–216.
- (30) Cretich, M.; di Carlo, G.; Longhi, R.; Gotti, C.; Spinella, N.; Coffa, S.; Galati, C.; Renna, L.; Chiari, M. *Anal. Chem.* **2009**, *81*, 5197–5203.
- (31) Auroux, P.-A.; Koc, Y.; deMello, A.; Manz, A.; Day, P. J. R. *Lab Chip* **2004**, *4*, 534–546.
- (32) Servoli, E.; Feitsma, H.; Kaptheijns, B.; van der Zaag, P. J.; Wimberger-Friedl, R. *Lab Chip* **2012**, *12*, 4992.
- (33) Squires, T. M.; Messinger, R. J.; Manalis, S. R. *Nat. Biotechnol.* **2008**, *26*, 417–426.
- (34) Nauwelaers, D.; Vijgen, L.; Atkinson, C.; Todd, A.; Geretti, A. M.; Van Ranst, M.; Stuyver, L. *J. Clin. Virol.* **2009**, *46*, 238–243.
- (35) SantaLucia, J.; Hicks, D. *Annu. Rev. Biophys. Biomol. Struct.* **2004**, *33*, 415–440.
- (36) Biancotto, A.; Wank, A.; Perl, S.; Cook, W.; Olnes, M. J.; Dagur, P. K.; Fuchs, J. C.; Langweiler, M.; Wang, E.; McCoy, J. P. *PLoS One* **2013**, *8*, e76091.
- (37) Quinn, J.; Gratalo, D.; Haden, K.; Moon, J. Accurate multiplex cytokine assay developed with VeraCode® technology. http://res.illumina.com/documents/products/whitepapers/whitepaper_veracode_cytokine_carboxyl.pdf.
- (38) Chowdhury, F.; Williams, A.; Johnson, P. J. *Immunol. Methods* **2009**, *340*, 55–64.
- (39) Dabitaio, D.; Margolick, J. B.; Lopez, J.; Bream, J. H. *J. Immunol. Methods* **2011**, *372*, 71–77.
- (40) Luminex Performance Human Cytokine Panel A. <http://www.rndsystems.com/Products/LUH000>.
- (41) Toedter, G.; Hayden, K.; Wagner, C.; Brodmerkel, C. *Clin. Vaccine Immunol.* **2008**, *15*, 42–48.
- (42) Joshi, R. V.; Zarutskie, J. A.; Stern, L. J. *Biochemistry* **2000**, *39*, 3751–3762.
- (43) Edwards, P. R.; Leatherbarrow, R. J. *Anal. Biochem.* **1997**, *246*, 1–6.
- (44) Cancer, T.; Atlas, G. *Nature* **2012**, *490*, 61–70.
- (45) Volinia, S.; Croce, C. M. *Proc. Natl. Acad. Sci. U. S. A.* **2013**, *110*, 7413–7417.